Breathing in thin air: structure, function and therapeutic opportunities of bd type oxidases

Velden, T.T. van der

Chapter 5

Towards a new cytochrome *bd* heme incorporation mechanism by direct complex formation between CydA and CydDC

Respiration is one of the principial processes that drives bioenergetics across the tree of life. In aerobic conditions, one of the central steps is the enzymatic reduction of molecular oxygen to water, catalyzed by the terminal oxidases. A subclass of these enzymes are the *bd*-type oxidases (cyt *bd*), solely found in prokaryotes and characterized by their heme-only oxygen reduction site. The incorporation of these hemes into cyt *bd* is a multistep process crucial for its oxidase activity. Recent studies have identified the type IV ATP-binding cassette (ABC) transporter CydDC as a key factor in heme delivery to cyt *bd*. However, the molecular mechanism by which heme transported across the cytoplasmic membrane is incorporated into cyt *bd* remains unresolved. Here, we combine protein purification, spectroscopy, mass spectrometry, cryo-electron microscopy and structure prediction to investigate potential interactions between CydDC and the CydA subunit of cyt *bd*. In *E. coli*, AlphaFold 3 predictions identify a high-confidence interaction interface between CydDC and CydA, suggesting direct complex formation. Fingerprinting analysis and cryo-EM are consistent with the presence of CydA in CydC pulldown samples. However, limited resolution and sample heterogeneity preclude unambiguous structural assignment. Based on these observations and structural predictions, we propose a putative model in which lateral association of CydDC with CydA enables direct heme transfer via a lateral gate formed between CydC helix 2 and CydD helix 5. This mechanism could allow direct heme incorporation during cyt *bd* maturation without a previously proposed periplasmic shuttle protein. Future experiments are proposed to further assess this model. Elucidating this pathway provides new insight into respiratory oxidase maturation and may reveal novel targets for antimicrobial intervention.

Introduction

Aerobic respiration is one of the main biochemical processes that drives ATP generation across the tree of life. During this process, the enzyme class of respiratory oxidases reduce molecular oxygen to water, often displacing protons across the inner membrane to create a proton motive force required for ATP synthesis. Evolution has resulted in three distinct types of these respiratory oxidases based on their active site architecture. These include the heme-copper oxidases, characterized by a heme-copper active site, the alternative oxidases, characterized by an iron-iron active site, and the *bd* oxidases, which utilize a heme *d* co-factor to catalyze the four-electron reduction of oxygen to water.

The *bd*-type oxidases are particularly notable for their role in energy conservation under microaerobic and stress conditions, highlighted by their remarkable affinity for oxygen[46,47]. The *bd* oxidases are selectively found in prokaryotes, and in pathogens contribute to virulence, antibiotic resistance, and oxidative stress tolerance[48,58,59,112]. Structurally, *bd* type oxidases consist of two core subunits, CydA and CydB, with additional small subunits such as CydX and CydH found in some species including *E. coli* cytochrome *bd*-I (*Ecbd*)[83]. The CydA subunits harbors three heme groups required for catalysis, while the CydB unit is hypothesized to have a structural role providing stability to the complex[91]. In *E. coli*, a secondary *bd* oxidase, cyt *bd*-II, resembles the cyt *bd*-I architecture including its heme cofactors, although being expressed at near-anaerobic conditions to maintain respiration when the bo_3 and *bd*-I oxidase lack oxygen affinity[87,144]. The assembly and function of *bd* oxidases depends on a multistep process that requires coordinated integration of the characteristic heme cofactors into the CydA subunit, a process that remains incompletely understood.

Central to this process is the type IV ATP-binding cassette (ABC) transporter CydDC, a heterodimer composed of CydD and CydC subunits. Genetic studies have shown that CydD and CydC often are adjacent on the same operon as cyt *bd*[95], and that deletion of CydD or CydC leads to loss of the characteristic cyt *bd* heme signal and oxidase activity[196]. CydDC has been proposed to export

low-molecular-weight thiols such as glutathione and cysteine, thereby modulating the redox environment of the periplasm[95]. However, emerging evidence indicates a direct role in heme transport[197,198], raising fundamental questions how the heme transported by CydDC gets incorporation into cyt *bd*.

Despite its importance, the molecular mechanism by which CydDC contributes to cyt *bd* assembly has remained elusive. Biochemical and structural studies have shown heme binding and displacement into the core of the CydDC transmembrane domain[198]. The heme release mechanism of CydDC, however, remains speculative. Molecular dynamics simulations indicate a rapid opening of the CydDC gate towards the periplasm, allowing the release of heme[198]. Current hypotheses point to an unknown periplasmic partner protein that can shuttle the exported heme from CydDC to CydA to form mature cyt *bd*[197,198], although direct evidence for this hypothesis is lacking. Heme transport and enzyme maturation are key to respiration and given its potential as a target for antimicrobial intervention, resolving the heme incorporation mechanism by CydDC is of great interest.

Here, we explore the alternative hypothesis that CydDC directly associates with the CydA subunit during cyt *bd* biogenesis. Using structural predictions and experimental approaches, we investigate whether transient CydDC–CydA (CydADC) complex formation could enable direct heme transfer into the CydA core.

Results

Co-evolution of CydA and CydDC indicates a common binding interface

The genes for cyt *bd* and CydDC are adjacent on the *E. coli* genome, although they are regulated under distinct promotors (Fig. 5.1A)[199,200]. Expression analysis indicates coordinated expression between CydDC and both *E. coli* cyt *bd* oxidases (*bd*-I: CydA, CydB ; *bd*-II: AppA, AppC), lacking coordination with the bo_3 oxidase (CyoA, CyoB)[201], hinting at a correlated functional role

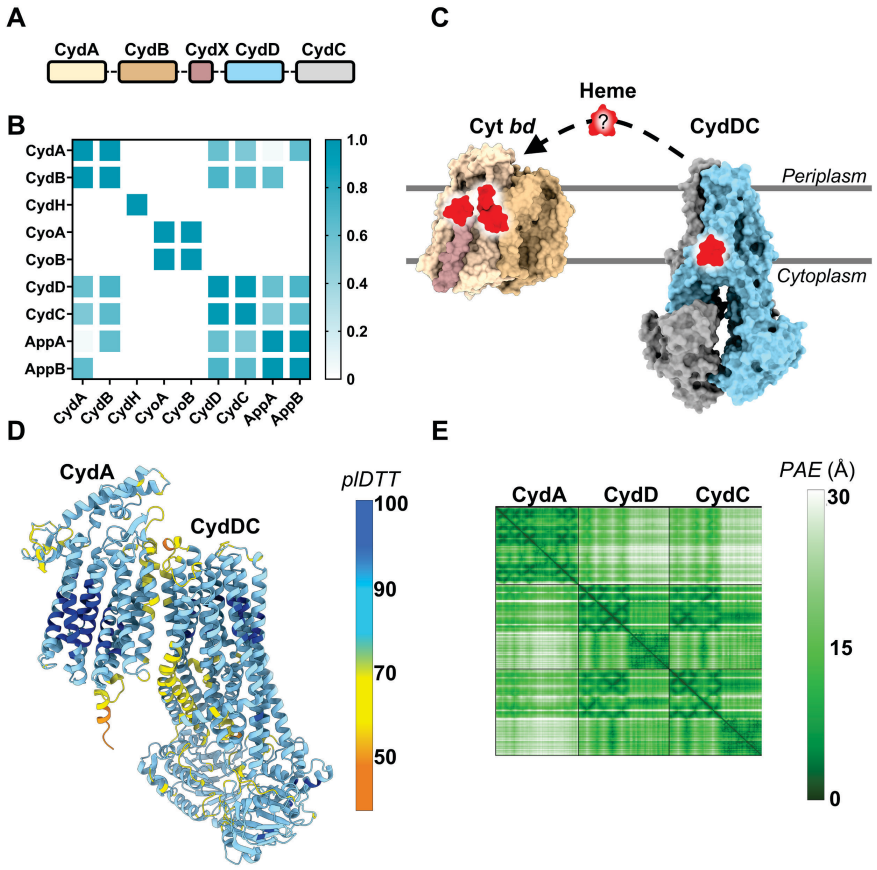

Figure 5.1 (**A**) Genomic organization of *E. coli* cyt *bd*, CydA, CydB, CydX and CydDC. (**B**) Co-expression of the cyt *bd* and CydDC subunits according to the STRING database[201] (**C**). Proposed heme incorporation mechanism, highlighting an unknown periplasmic chaperone to transfer the heme from CydDC to cyt *bd* [197,198]. (**D**) AlphaFold 3 prediction of the CydA and CydDC subunits, colored by plDTT with its associated (**E**) PAE plot.

in *bd* oxidase maturation (Fig. 5.1B). Recent advances in the CydDC heme transport mechanism hypothesize that a periplasmic partner protein shuttles the exported heme through the periplasm into the CydA subunit of cyt *bd* [197,198] (Fig. 5.1C). To study this heme incorporation mechanism of CydDC into CydA, an AlphaFold 3 interactome study was performed. Surprisingly, AlphaFold 3 prediction indicates a stable complex between CydA subunit and CydDC in the absence of CydB in *E. coli* (Fig. 5.1D,E), and across several other species (Fig.

S5.1). These predictions suggest that CydDC may transiently associate with CydA, potentially enabling direct heme transfer prior to full cyt *bd* assembly.

Purification of a putative CydADC complex

To probe the existence of a CydA-CydDC (CydADC) complex, we have cloned the CydDC genes into the pET17bCydABX-linkerstrep plasmid. During cloning, CydDC with a C-terminal His tag on CydC was used to replace the CydB to enable affinity purification of the transporter. The removal of the CydB subunit was performed to minimize binding competition for CydA after heme incorporation by CydDC (Fig. 5.2A, Fig. S5.1). This plasmid was transformed into BL21 Rosetta cells and expressed overnight in M9 minimal media. The protein was purified using IMAC affinity purification of the CydC subunit followed by gel filtration to study the pulldown of CydA. SEC MALS analysis of the purified complex indicates the existence of multiple oligomeric species, as indicated by a shoulder of the main peak with increasing molecular weight between 200 and 400 kDa (Fig. 5.2B). The purified protein showed clear bands for both the CydC and CydD subunits, as confirmed by western blot (Fig. 5.2C). Additionally, a faint band was observed at the molecular weight of CydA. To provide indirect evidence of CydA binding, a western blot against the strep tagged CydX was performed, which specifically associates with CydA in the mature cyt *bd* complex[83]. This indicates co-purification of the CydX subunit, suggesting the presence of CydA after CydC pulldown (Fig. 5.2C).

To detect the presence of specific heme species in the purified protein preparation, a reduced minus oxidized UV-vis spectrum was taken. This difference spectrum shows signals corresponding to the presence of *b*-type hemes, without a clear heme *d* signature as is observed in mature *Ecbd* (Fig. 5.2D). This indicates that if CydA is bound to CydDC, it has not yet fully matured its heme *d* oxygen reduction site. Additionally, it should be noted that purified CydDC has previously been shown to contain a heme signal corresponding to heme *b* [202], which means that no heme signal can unambiguously be assigned to CydA. Mass spectrometry-based fingerprinting following trypsin digestion detected significant enrichment of CydA in comparison

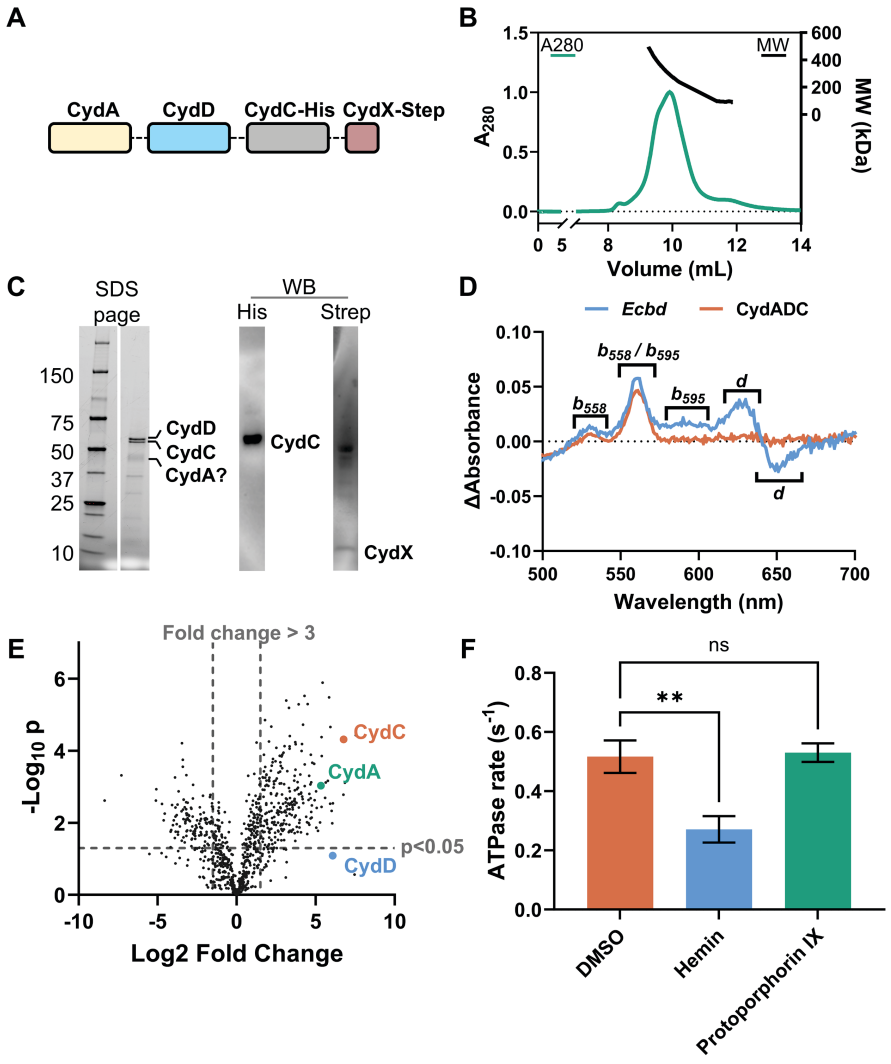

Figure 5.2 Purification and characterization of the putative CydADC complex. (**A**) Organization of genes and purification tags in the CydADC expression construct. (**B**) SEC-MALS analysis of the purified complex. (**C**) SDS page and western blot against CydC (His) and CydX (Strep). (**D**) Reduced minus oxidized UV vis spectrum of the purified complex in comparison to purified *Ecbd*. Data is normalized to the Soret band (417 nm) in the oxidized spectrum (20 mM MES pH 6.0, 50 mM KCl, 0.001% LMNG). (**E**) Fingerprinting results of the purified complex (N=3), indicating the presence of CydA. (**F**) ATPase activity of the purified complex (N=2), inhibited upon exposure to hemin (20 mM Tris-HCl (pH 7.0), 50 mM KCl, 4 mM $MgCl_2$, 350 µM PEP, 350 µM ATP, 350 µM NADH, 2.5 v/v% pyruvate kinase and lactate dehydrogenase solution (ThermoFisher), 0.002% LMNG, 500 nM substrate in DMSO, 80 µg/mL purified transporter (final 1 v/v% DMSO).

to a negative control (his-tagged purified *C. thermarum* NDH2), providing additional, albeit indirect, evidence for complex formation (Fig. 5.2E). The purified preparation showed ATPase activity indicating functional integrity of the transporter (Fig. 5.2F). Interestingly, exposure to hemin decreased the ATPase activity, an effect not seen with protoporphyrin IX. This indicates a kinetic profile that differs to previously characterized CydDC[197,198], and might indicate a specific effect the iron containing hemin has on the putative CydADC complex.

Cryo-EM and structure prediction of the CydADC complex

To further explore the existence of the putative CydADC complex, we performed cryogenic electron microscopy (cryo-EM) on the purified transporter sample. The sample was concentrated to 1.5 mg/mL and blotted on a 300 mesh copper grid. A total of 7408 movies were collected on a titan Glacios microscope at 50 $e^-/Å^2$ and a 0.88 Å calibrated pixel size (Fig. 5.3A). The movies were imported into CryoSPARC live and subjected to patch-based motion correction followed by blob picking, multiple rounds of 2D classification, and finally unsupervised *ab-initio* model generation (Fig. 5.3B). Data collection and image processing revealed a dominant particle population corresponding to CydDC in a conformation consistent with previously solved structures. These particles displayed well-defined side and top views characteristic of the CydDC heterodimer[197,198] (Fig. 5.3C). A smaller subset of particles exhibited an asymmetric detergent micelle and additional lateral density. *Ab-initio* reconstruction of this subset revealed density compatible with a three-subunit CydADC assembly. However, the resolution and structural definition were insufficient to confidently assign the additional density to CydA (Fig. 5.3D). These results suggest that if a CydADC complex exists, it is likely transient, low-abundance, or structurally heterogeneous, precluding unambiguous visualization under the conditions tested.

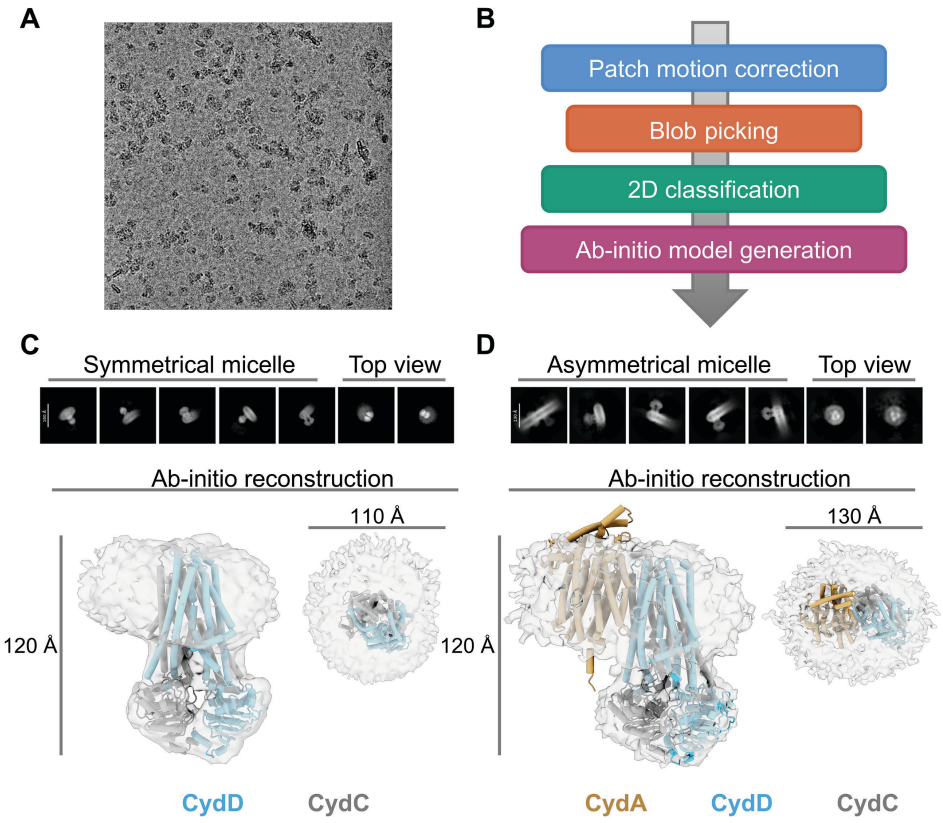

Figure 5.3. (**A**) Representative micrograph of the collected dataset (**B**) Schematic data processing strategy in CryoSPARC (**C**) Selected 2D classes and corresponding ab initio volume of the CydDC complex. (**D**) Selected 2D classes and ab initio volume of the putative CydADC complex, highlighted by an assymetical micelle and threefold density seen from the top.

Discussion

Recent advances in the structure and function of CydDC have highlighted a clear relationship with the heme maturation mechanism cyt *bd*. Despite extensive research into the heme transport mechanism of CydDC, no experimental evidence has shown how heme is released from CydDC for downstream incorporation into cyt *bd*. Existing models invoke periplasmic heme release and capture by an unidentified shuttle protein, despite the absence of direct experimental evidence[197,198]. Using structural predictions of AlphaFold 3, we hypothesize that CydDC can bind laterally to the CydA subunit during cyt *bd* maturation, allowing for direct heme incorporation without the need for an additional binding partner. After heme incorporation, the CydA subunit would be released from CydDC, and subsequently stabilized by binding to the CydB, CydX and CydH subunits.

Co-expression and purification of CydA and CydDC shows to contain species of varying molecular weight, with an additional faint band at the molecular weight of CydA indicating the presence of multiple purified protein complexes. Western blot and protein fingerprinting underline co-purification of CydA and CydX, suggesting complex formation. Heme analysis, however, show the absence of the characteristic *d*-type heme signal, indicative of incomplete maturation of the co-purified CydA subunit. The complex purified here shows significant inhibition rather than stimulation of ATPase activity upon exposure to substrate hemin. Similar decreases in ATPase activity have been observed for the *E. coli* methionine and *Methanosarcina acetivorans* molybdate transporter upon exposure to its substrate and was attributed to the stabilization of a state which decreases futile ATP hydrolysis[203,204]. The decrease in ATPase activity observed here is in stark contrast with previously characterized CydDC, suggesting a change in heme handling[197,198]. Regretfully, our purified protein complex was shown to be heterogenous, prohibiting direct comparison of transporter kinetics with a single protein state. Potentially, the subpopulation existing as a CydADC complex exhibits an altered structural landscape upon binding to heme, explaining the distinct kinetic response upon heme exposure. However, due to the sample heterogeneity, unambiguous conclusions cannot be made. Furthermore, it should be noted that CydDC has

not yet been separately purified as a control to our experiments, warranting caution in interpretation of the characteristics presented here.

Interestingly, CydDC has not yet been probed for the transport of *d*-type hemes, the characteristic active site co-factor in cyt *bd*. Direct transport of this heme subtype by CydDC would be interesting as current discussions propose the formation of *d*-type hemes *in situ* after incorporation of a *b*-type heme into its host protein[205,206]. Heme *d* is formed by lactone formation of the propionate group of heme *b*, introducing a chiral carbon on the porphyrin ring of heme *d*, presenting both cis and trans variants. If heme *d* formation occurs *in situ*, this could indicate why different heme *d* chirality's are reported in cyt *bd* oxidases[153,192], potentially imposed by the local environment during lactone formation. Whether heme *d* chirality affects cyt *bd* activity remains to be determined.

Regretfully, despite biochemical indications of CydA co-purification, cryo-EM analysis was unable to produce explicit structural features in line with the CydADC complex. Potentially, the CydA subunit rapidly releases from CydDC after heme incorporation, hindering stable complex formation for purification and structural integration. Regardless, the structure of CydADC predicted by AlphaFold 3 provides a putative framework for proposing a mechanistic model of heme incorporation. The model suggests that lateral association of CydDC with the CydA subunit forms a transient assembly that enables direct heme transfer without the requirement for an additional periplasmic carrier protein. In this configuration, heme bound to CydDC in the previously described heme-confined state[196,197] must first be repositioned toward the midplane of the membrane through the transmembrane helices of CydDC. Upon reaching this membrane-embedded position, the cofactor can be inserted laterally into CydA, allowing sequential incorporation of all three heme groups (Fig. 5.4A). Notably, this model diverges from earlier proposals suggesting periplasmic release. Instead, it requires formation of a lateral gate in the outward-open conformation of CydDC. We propose that this gate is formed at the interface between helix 2 of CydC and helix 5 of CydD and opens upon ATP binding to the CydC NBD. A laterally open conformation has not been observed in molecular dynamics simulations of *E. coli* CydDC[197,198], however, such a state may be

stabilized only in the presence of CydA, which was absent in previous simulations. Interestingly, CydDC from *M. smegmatis* has been solved in an outward open state using cryo-EM[197]. This state shows the formation of a lateral gate between helix 1 and 6 of CydC, as well as helix 5 of CydC and helix 2 of CydD[197]. This lateral opening in CydDC is directly opposite to the CydADC interface in our predicted structures (Fig. S5.2). While this argues against the model proposed here, the structural landscape of CydDC potentially changes upon binding to CydA, allowing for the opening of the lateral gate between CydC helix 2 and CydD helix 5 for direct heme incorporation. Notably, lateral gate opening has precedent in other type IV ABC transporters, including the lipid flippase MsbA[207], supporting the mechanistic plausibility of intramembrane heme transfer.

Assuming this lateral docking model is correct, a stepwise mechanism of heme incorporation can be derived (Fig. 5.4B). During assembly of cyt *bd*, CydA initially associates laterally with CydDC. In the inward-open state of CydDC, heme binds within the transmembrane region. Release of ADP from the CydC NBD promotes translocation of heme into the central cavity, corresponding to the heme-confined state[198]. Subsequent ATP binding induces conformational rearrangements that drive heme toward the transmembrane mid membrane plane and trigger opening of the proposed lateral gate between CydC and CydD, thereby establishing direct access to CydA. Following ATP hydrolysis, CydDC returns to the inward-open state, resetting the transporter for another cycle. This process is repeated three times to achieve complete incorporation of the three heme cofactors into CydA. Upon completion, CydA disengages from CydDC and stabilizes its structure through association with CydB, CydH and CydX. Formation of the mature cyt *bd* complex then enables initiation of respiratory activity.

Future studies are required to unambiguously prove the formation of the CydADC complex. Most likely, this requires optimization of the expression and purification protocol to isolate the intact complex. Stabilization strategies, such as ATPase-inactive CydDC mutants ($H85A^{CydC}$ or $E500Q^{CydC}$), chemical crosslinking, dual-affinity purification of CydDC and CydA, or cell-free co-expression, may facilitate stable complex purification for future

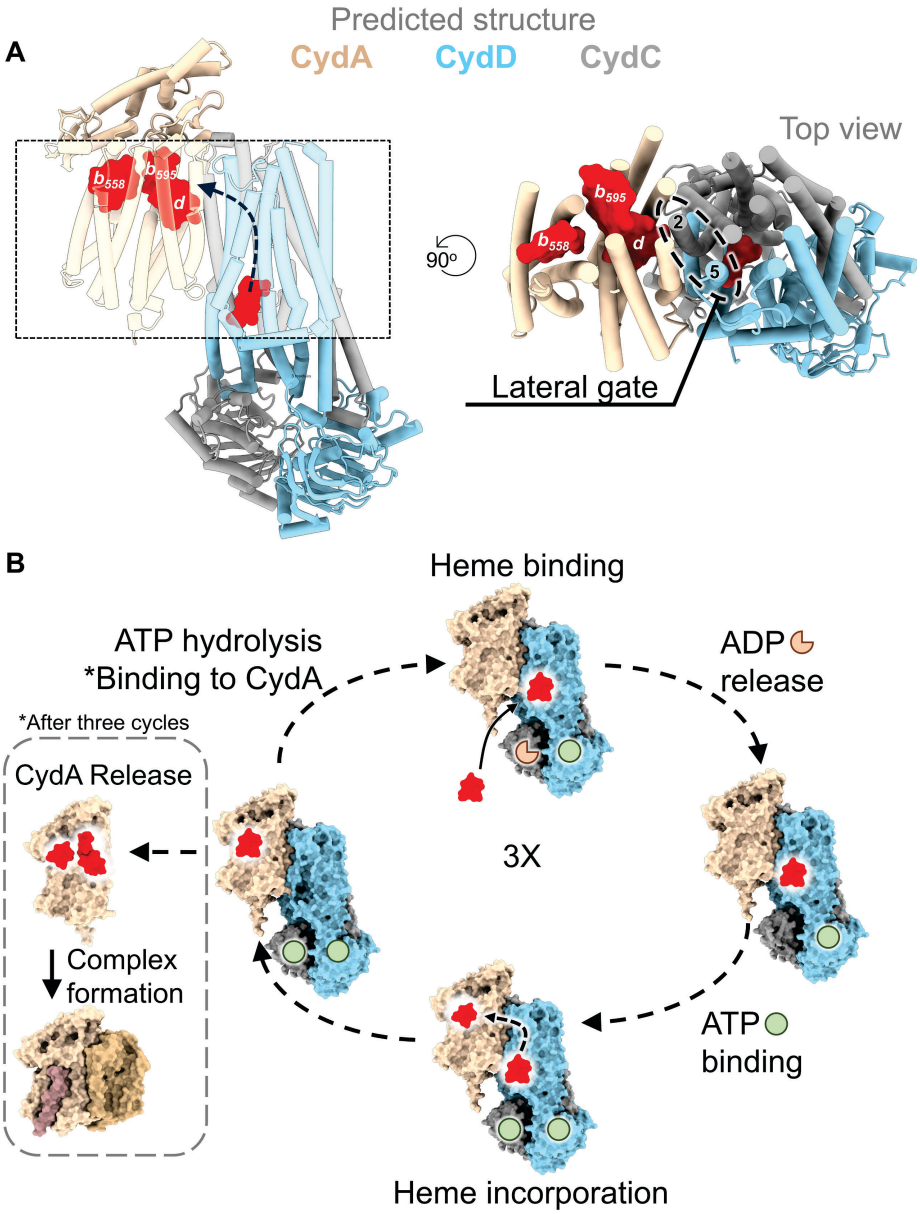

Figure 5.4 (**A**) Representation of the putative heme transport pathway in the CydADC complex, moving the heme from the confined state in CydDC into the CydA subunit. This mechanism would require the opening of a lateral gate between helix 2 of CydC and helix 5 of CydD. (**B**) Putative heme incorporation mechanism based on the predicted CydADC complex.

structural characterization. Alternatively, genome wide analysis of co-expression or an interactome studies using proximity-based MS labeling might point to CydDC binding partners, whether this is CydA or an unknown binding partner. Additionally, reliable control samples are needed, both CydDC for kinetic evaluation, and non-CydA interacting alternatives for pulldown, to validate the overall biochemical evaluation. Solving the heme transport of CydDC and heme incorporation mechanism into cyt *bd* provides fundamental information into the maturation of this important class of enzymes and provides further foundation for antibiotic development targeting microbial respiration.

Experimental procedures

Cloning and mutagenesis

The CydDC gene with a hexahistidine tag on the CydC C-terminus was ordered from Genscript and cloned into the pET17bCydABXlinkerstrep plasmid, exchanging the CydB gene for CydDC using Gibson assembly (Fig. S5.1). The newly created pET17BCydADCHis construct was confirmed using nanopore whole plasmid sequencing.

Expression and purification of the CydA-CydDC complex

The pET17BCydADCHis was transformed into *E. coli* BL21 Rosetta and incubated overnight at 37°C to select positive transformants. Expression and purification were based on prior CydDC purifications[198]. A streak of colonies was inoculated in LB supplemented with 100 µg/mL ampicillin and grown overnight at 37°C, 200 rpm. The culture was diluted 1:100 in M9 media (100 ug/mL ampicillin) and grown to OD 0.8. Prior to induction, the culture was cooled to 16°C followed by addition of 1 mM IPTG. The CydADC complex was expressed for 16 hours before harvesting (7540 rcf, 20 min, 4°C). Cells were resuspended in 20 mM Tris-HCl, 300 mM NaCl, 100 mM KCl, 4 mM $MgCl_2$, pH 8.0, cOmplete protease

inhibitor before lysis using and Stansted cell homogenizer operating at 270 MPa. Cell debris were pelleted (10.000 rcf, 20 min 4°C) before membrane harvesting (200.000 rcf, 1h, 4°C). Membranes were resuspended in 20 mM Tris-HCl, 300 mM NaCl, 100 mM KCl, 4 mM $MgCl_2$, pH 8.0 and adjusted to a total protein concentration of 10 mg/mL as determined by BCA assay (ThermoFisher). Solubilization of the membrane protein was achieved by addition of 0.5% LMNG and gentle mixing for 1 hour at 4°C. Remaining insoluble materials were pelleted (200.000 rcf, 1h, 4°C) before application of the soluble fraction on a 5mL Hitrap Talon column (Cytiva). Sample application was performed at 0.5 mg/mL, following a wash of 10 column volumes using 20 mM Tris-HCl, 300 mM NaCl, 100 mM KCl, 4 mM $MgCl_2$, 10% glycerol, 0.002% LMNG, pH 8.0 at 1 mL/min. Sample elution was achieved using a linear gradient from 0 to 240 mM imidazole over 40 column volumes. Peak fractions were pooled and further purified using gel filtration using a Superdex 10/300 200 column at 0.5 mL/min (20 mM MES pH 6.0, 50 mM KCl, 0.001% LMNG). Peak fractions were pooled, concentrated and stored at -80°C until further use.

Reduced minus oxidized UV vis spectroscopy

Heme content of the purified transporter was analyzed using an oxidized minus reduced UV vis spectrum. CydADC was oxidized with 0.25 mM hexacyanoferrate in 20 mM MES pH 6.0, 50 mM KCl, 0.001% LMNG, and reduced by adding a few grains of sodium dithionite. Specific heme reduction was found by subtracting the oxidized from the reduced spectrum. The spectra were normalized to the Soret band at 417 nm of the respective oxidized spectra.

SEC-MALS analysis

The CydADC sample (1 mg/mL) in LMNG detergent was injected and characterized on a SEC-MALS system running 50 mM Tris HCl, 200 mM NaCl, 0.005% LMNG at 0.5 mL/min. The system was comprised of a miniDAWN® TREOS®, Optilab differential refractometer (Wyatt technology) and 1260 Infinity II multiple wavelength absorbance detector (Agilent).

ATPase activity

ATPase activity of the purified transporter was performed as described previously[198]. Briefly, heme substrates were dissolved in DMSO and added (500 nM final concentration) to the ATPase activity buffer when required (20 mM Tris-HCl (pH 7.0), 50 mM KCl, 4 mM $MgCl_2$, 350 µM phosphoenolpyruvate (PEP), 350 µM ATP, 350 µM NADH, 2.5 v/v % of pyruvate kinase and lactate dehydrogenase enzyme solution (Sigma Aldrich), 0.002% LMNG). This mix was preheated for 5 minutes in a FLUOstar platereader set to 37°C prior to the addition of 80 µg/mL purified transporter. ATPase activity was measured for 60 minutes by determining the coupled NADH oxidation rate (340 nm).

Protein fingerprinting

To establish the presence of CydA in the CydADC pulldown, purified protein was subjected to fingerprinting. To control for aspecific co-purification of CydA, His purified *C. thermarum* NDH2 (as previously described[159]) was used as a control. Each protein sample was precipitated in 80 vol/vol% ice cold acetone at 5 ug total protein and stored at -20°C for one hour. Subsequently, the precipitated protein was pelleted by centrifugation at 4000 g for 10 min, followed by removal of the supernatant. The protein pellet was resuspended in 8M urea and incubated at 37°C for 30 minutes while shaking to achieve protein denaturation. Subsequently, 3.1 mg/mL DTT was added for disulfide bond reduction and incubated at 37°C for 15 minutes. The reduced cysteines were capped by addition of iodoacetamide (7.4 mg/mL) and incubation at 37°C for 30 min. Proteins were digested using 200 ng trypsin (ThermoFisher) and incubated overnight at 37°C. The following day, C18 silica stage tips were prepared by washing with methanol, followed by 0.5% (vol/vol) formic acid (FA) in 80% (vol/vol) acetonitrile (ACN)/MilliQ and 0.5% (vol/vol) FA in MilliQ. Digested protein samples were loaded onto the stage tips by centrifugation (400 rcf). After loading, the stagetips were washed with 0.5% (vol/vol) FA in MilliQ, followed by elution into fresh low binding tubes using 0.5% (vol/vol) FA in 80%

(vol/vol) ACN/MilliQ. The samples were evaporated to dryness using a speedvac (45°C), followed by freshly dissolving into 0.1% TFA in MilliQ prior to Mass spec injection.

Peptides were separated via nanoflow reversed-phase liquid chromatography using a Vanquish Neo UHPLC system setup in a trap-elute configuration. For trapping peptides, a PepMap Neo 5 µm C18, 300 µm x 5 mm trap (Thermo Scientific, 174500) was used which was eluted into an Easy-Spray PepMap Neo 2 µm C18, 75 µm x 500 mm analytical column (Thermo Scientific, ES75500PN) kept at 50°C with a constant flowrate of 0.3 µL/min. The mobile phase consisted of a mixture of mobile phase A (0.1% FA in ULC-MS grade water (Biosolve) and mobile phase B (0.1% FA in 80% ULC-MS grade acetonitrile (Biosolve), and the separation was performed with a gradient from 4 – 44% B over 40 min, followed by an increase to 90% B over 5 min and a column wash with 90% B for 14 min before column re-equilibration. Peptides were introduced to an Orbitrap Eclipse Tribrid Mass Spectrometer (Thermo Scientific) with a spray voltage of 1.5 kV. Data was acquired in data-dependent acquisition (DDA) mode with the following scan sequence: MS1 master scan (Orbitrap analysis, 240K resolution, 375-1500 m/z, RF lens 30%, 80 ms maximum injection time) with dynamic exclusion enabled (repeat count 1, exclusion duration 60 s, mass tolerance 10 ppm, dependent scan on single charge state per precursor only). The top precursors were then selected for MS2 analysis with an intensity threshold of 1.0 E4 within a 1.7 second duty cycle through quadrupole isolation (1.2 m/z isolation window) followed by higher-energy collisional dissociation in the ion routing multipole (normalized collision energy 30%) and analysis of the resulting fragments in the orbitrap (15K resolution, 100 ms maximum injection time, centroid mode). The data was searched using FragPipe v23.1 used using the pre-defined workflow LFQ-MBR[197]. A database was created by adding reverse entries to reviewed human proteome (Uniprot, February 2025, 20402 entries) supplemented with a list of contaminant proteins[200] . MSFragger[208,209] (version 4.3) was used to search DDA-PASEF data using the default settings. In the validation step, MSBooster (version 1.1.11) was implemented on both spectra and RT levels, and subsequently Percolator[210] and ProteinProphet[211] integrated in Philosopher (version 5.0.0) were used for

PSM validation and protein inference. Quantification was performed by IonQuant[212] (version 1.11.11) using proteotypic peptides only. Normalization was turned off.

Cryo-EM Sample Preparation and Data Collection

C-flat R1.2/1.3 grids (mesh 300) were glow discharged with a PELCO easiGlow device at 15 mA for 90s. CydADC in LMNG (4 µL, 1.5 mg/ml) was applied to the grid, followed by blotting at 4°C, 100% humidity, 10 blot force for 4 seconds using a Vitrobot IV device (Thermo Fisher) immediately before plunge freezing in liquid ethane.

Grids were imaged on a Titan Glacios (ThermoFisher Scientific) operating at 200 kV with a Falcon 4i detector and selectris energy filter with a slit width of 20 eV. Movies were gathered in electron counting mode using aberration-free image-shift (AFIS) in EPU (ThermoFisher Scientific). A total dose of 50 $e^-/Å^2$ at 130,000× magnification with a calibrated pixel size of 0.880 Å, at and a defocus range of -1.0 to -2.0 µm.

Cryo-EM Data analysis

Data processing was performed in CryoSPARC. Image preprocessing was performed in CryoSPARC live[150] using Patch Motion Correction and Patch CTF estimation. The processed micrographs and particles were exported to CryoSPARC for further processing. Initial particle picking was performed with blob picking, followed by template generation for ABC transporter additional density in the micelle. Template particle picking was performed followed by multiple rounds of 2D classification to remove junk particles. Three volume unsupervised ab initio model generation was performed to generate initial and bait volumes for further particle cleanup. Further rounds of heterogeneous refinement were performed but did not yield improvements in the density of CydDC.

AlphaFold prediction and model analysis

The CydADC complex was predicted using the AlphaFold 3 servers using different combinations of the CydC, CydD, CydA and CydB subunits from various species. To visualize heme binding pockets, the predicted CydADC complex was aligned to known structures of cytochrome *bd*(6RKO) and CydDC (7ZDG). Models and ab initio Cryo-EM maps were assessed and analyzed in ChimeraX[176] (version 1.7.1).

Author contributions

All experiments were performed by T.T van der Velden. Mass spec data collected was performed by B. Gagestein from the mass spec facility. The chapter was written by T.T. van der Velden under the supervision of L.J.C Jeuken.

Supplementary information

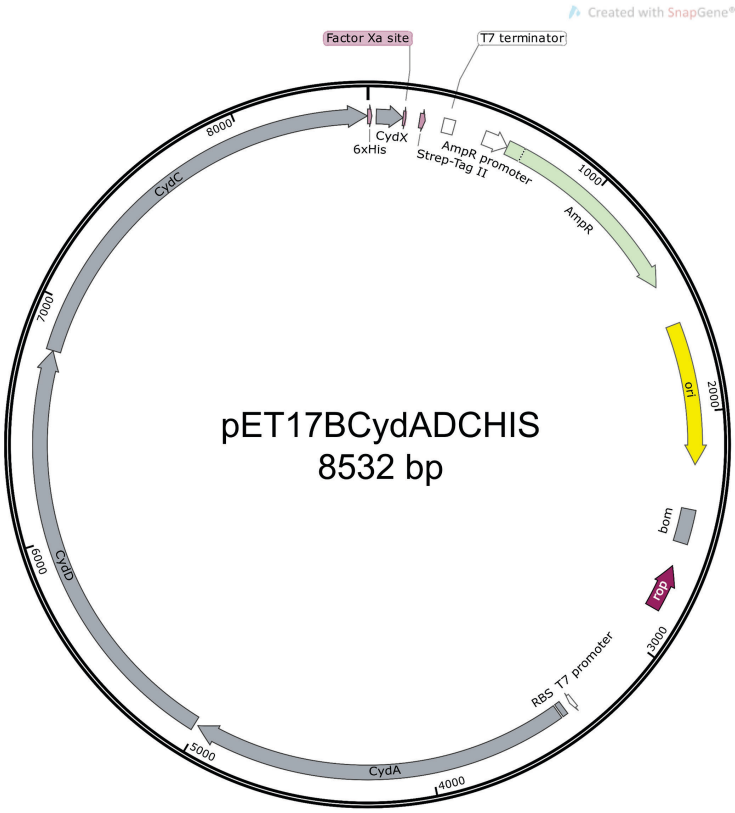

Figure S5.1. Plasmid map of the pET17BCydADCHis expression construct.

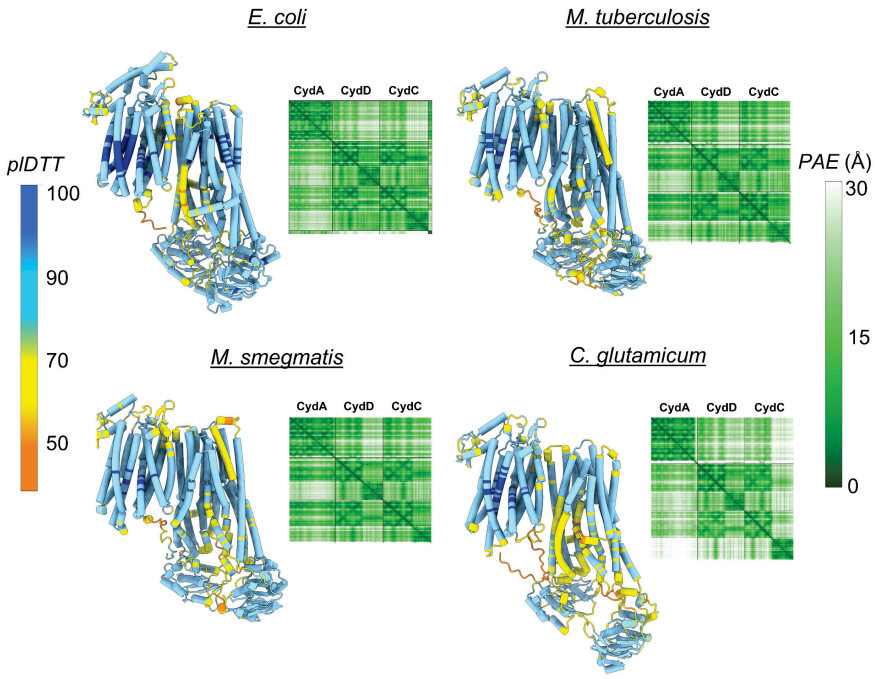

Figure S5.2. Alphafold prediction of the putative CydADC complex from *E.coli*, *M. tuberculosis*, *M. smegmatis*, and *C. glutamicum*, colored by plDTT.

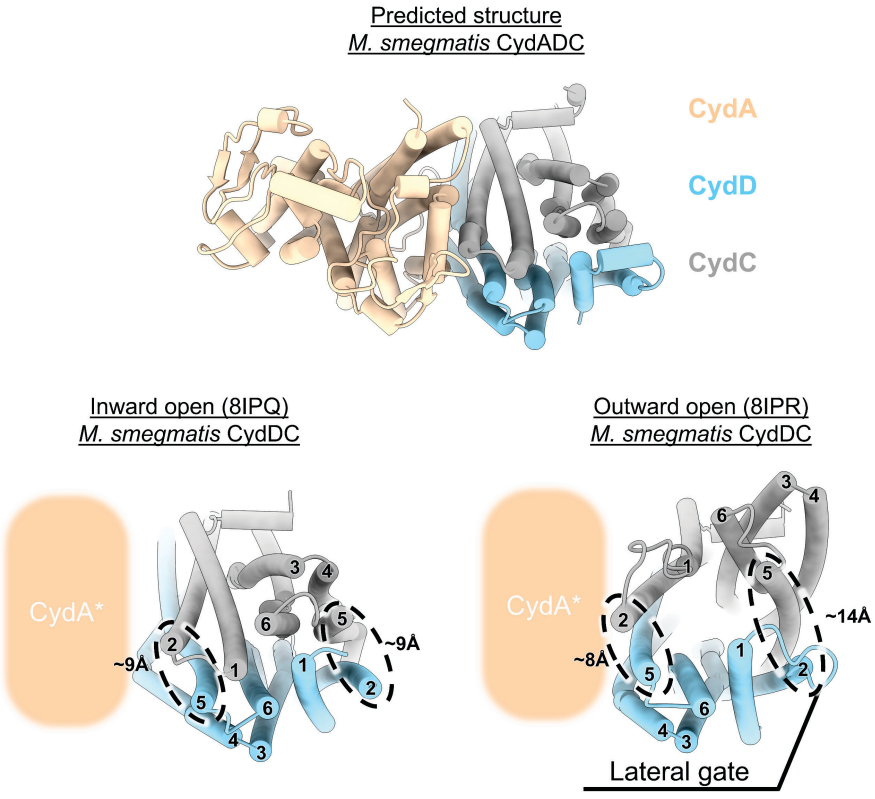

Figure S5.3. Top view of the predicted *M. smegmatis* CydADC complex in comparison with the solved cryo-EM structures of *M. smegmatis* CydDC in the inward (8IPQ) and outward (8IPR) open states.